Seasonal and Vertical Tidal Variability in the Southeastern Mediterranean Sea

Nadav Mantel[1], Yizhak Feliks[1], Hezi Gildor[1], Pierre-Marie Poulain[2], Elena Mauri[2], Milena Menna[2]

[1]The Institute of Earth Sciences, The Hebrew University of Jerusalem.

[2]Istituto Nazionale di Oceanografia e di Geofisica Sperimentale, OGS, Borgo Grotta Gigante, 42/c, 34010 Sgonico, Italy.

Corresponding author: Nadav Mantel (nadav.mantel@mail.huji.ac.il)

Key Points:

- We analyze long-term measurements of velocity and pressure that enable seasonal and depth analysis of tides in the Eastern Levantine Basin
- The observed UPS1 apparently results from leakage of near-inertial motion
- Velocity from drifters and moored datasets were compared and used to assess different time criteria for tidal and spectral analysis

Abstract

Currents and pressure records from the DeepLev mooring station (Eastern Levantine Basin) are analyzed to identify the dominant tidal constituents and their seasonal and depth variability. Harmonic and spectral analysis on seasonal segments of currents and pressure reveal attributes of the tidal regime in the Eastern Levantine Basin: (1) Dominant semidiurnal sea-level variability; (2) seasonal variation of semidiurnal and diurnal tides found in both currents and pressure datasets; and (3) significant diurnal currents with weak semidiurnal currents in all seasons. The most dominant tidal constituent found from the pressure dataset is the M2 (12.4 h). Results from pressure datasets generally agree with previous models and observations of semidiurnal tides, while the diurnal tides are larger than previously reported by 8-9 cm in the winter and 1-2 cm in the summer. The surface current variability differs from the one reported before in the Eastern Levantine Basin, with M2 magnitudes weaker by 1 cm, while the diurnal tides (K1, O1) are 1-2 cm larger. Seasonal segments showed seasonal differences in the local tidal regime's amplitudes, with the K1 (7 cm difference between winter and fall) and S2 (4 cm difference between summer and fall) the most pronounced. We analyzed the M2 and S2 tides using surface drifters near DeepLev at different dataset lengths while considering the time constraints needed to resolve the tides adequately. The longer the dataset, the higher the resolution of the tidal analysis and the lower the amplitude leakages from nearby frequencies resulting in weaker tidal currents.

Plain Language Summary

We examined the southeastern Mediterranean Sea tides, focusing on the Eastern Levantine Basin. Using data from a moored device located 50 km from the Israeli coast, recording pressure and currents from near surface to 1300 m depth and information from satellite-tracked surface drifters, we aimed to better understand tidal patterns in this region.

Our findings show (1) A prominent tidal elevation cycle occurring roughly every 12.4 hours. (2) Notable changes in tidal patterns across different seasons. For instance, the tides can be 8-9 cm higher in winter than in summer. (3) Significant daily tidal currents with weak twice-a-day currents in all seasons.

We noticed some differences when comparing data from fixed underwater devices and drifting ones. Drifters that collect data over longer periods give more detailed and accurate results. However, their movement across different areas can slightly alter the findings due to varying conditions.

Understanding these tidal patterns is crucial. It impacts several areas, from ensuring safer sea travel to understanding how pollutants spread in the water. Our study emphasizes the importance of using multiple data sources and considering time factors to comprehensively describe tidal variability.

1 Introduction

Tidal currents and tidal variations in sea level have attracted scholars for over 2000 years (see review by Deparis et al., 2013). Understanding tidal phenomena is essential for various practical applications, as these affect the dispersion of pollutants (Kar et al., 2022), larvae (Hsieh et al., 2010), the safety of marine transportation (Pastusiak, 2020), and more. In addition, numerical models are sensitive to the inclusion of tidal forcing (e.g., Naranjo et al., 2014;

Sannino et al., 2015). Tides in the Mediterranean Sea have been studied before, but only a few studies were conducted in the (deep part of the) Levantine Basin (summarized below). Here, we use long-term observations collected at the DeepLev mooring station in the Levantine Basin, hereinafter "DeepLev" (Katz et al., 2020), and satellite-tracked surface drifters to (1) identify the dominant tidal constituents in the Levantine Basin; (2) study the vertical and seasonal variability of the dominant constituents, and (3) compare the tidal constituents derived from moored current meters to those derived from surface drifters.

The Mediterranean is a semi-enclosed basin connected to the Atlantic Ocean by the Straits of Gibraltar, and it has a complex bathymetry. It is divided into two major basins by the Sicily Channel – the western basin and the eastern basin, and each basin includes many sub-basins, some shallow and some deep (Alberola et al., 1995; Gasparini et al., 2004). Thus, the characteristics of the tides can be different in different regions and depths (Poulain et al., 2018).

Tides in the Mediterranean were studied using both observations and models. Observations include current measurements from shipboard (Garcia-Gorriz et al., 2003; Gasparini et al., 2004), from moored instruments (Lafuente & Lucaya, 1994; Albérola et al., 1995; Ursella et al., 2014), using high-frequency (HF) coastal radars (Chavanne et al., 2007; Cosoli et al., 2015; Soto-Navarro et al., 2016), and using surface drifters (Poulain et al., 2007, 2013, 2015, 2018). In addition, numerical models with various complexities were also used to study tides in the Mediterranean Sea (e.g., Tsimplis et al., 1995; Arabelos et al., 2011).

A few previous studies identified four main constituents, M2, S2, K1, and O1 (e.g., Gasparini et al., 2004; Tsimplis et al., 1995; Cosoli et al., 2015; Sánchez-Román et al., 2018; Poulain et al., 2018), see Table 1 for the corresponding periods. Other studies identified and applied additional constituents in numerical models (Ferrarin et al., 2018; Arabelos et al., 2011). Differences in the dominant constituents at different locations are expected due to the complexity of the coastline and bathymetry.

There are specific constituents whose existence and importance need to be clarified, found in the tidal analysis, such as the diurnal UPS1 tide and the long fortnight Mf and Msf. Several observations at Alexandria have reported the presence of the UPS1 tide (El-Geziry & Radwan, 2012; El-Geziry, 2020; Khedr et al., 2018). 21.5-h oscillations, similar in the period to the UPS1 tide, were also observed at the Strait of Otranto (Ursella et al., 2014) and the Adriatic Sea (Medved et al., 2020). However, Ursula et al. (2014) and Medvedev et al. (2020) attributed this to the 21.5 h fundamental eigenmode in the Adriatic. At DeepLev, the inertial period is 21.99 h, while the UPS1 tide is 21.4 h. Therefore, a time series of roughly 49.85 days is needed to separate the two signals in a spectral analysis. Not only is the inertial period near the UPS1 in all the Eastern Mediterranean with a period between 20.5 h to 23.05 h affecting diurnal frequency analysis, but there are also shifts in the effective inertial frequencies due to background vorticity (Perkins, 1976; Kunze, 1985). Therefore, the inertial band in the Eastern Mediterranean may be misinterpreted as the UPS1 tide by spectral and tidal analysis even with a longer time series than 49 days.

Studies at the Strait of Gibraltar identified the existence of the Mf and Msf constituents (Tsimplis & Bryden, 2000; Millot & Garcia-Lafuente, 2011; Sammartino et al., 2015). These frequencies could be attributed to non-linear interactions between semidiurnal and diurnal tidal constituents in shallow seas and sea shelves (Kwong et al., 1997). However, the Mf and Msf constituents have also been observed in the Adriatic Sea (Chavanne et al., 2007; Vilibić et al., 2015) and the Marmara Sea (Ferrarin et al., 2018), and our results of the Msf tide have shown to be significant in a few of the analyzed datasets.

The seasonality of tides, and in particular, the seasonality of the M2 tide, has been studied both theoretically and experimentally. Müller et al. (2014) showed variations in the M2 tide in global models and tide gauge data from several areas worldwide, such as Victoria, Canada, and Cuxhaven, Germany. Müller et al. (2014) attribute the effects of stratification to the seasonality of the tides with the view that stronger stratification leads to less mixing and, hence, to less loss of kinetic energy of the barotropic tide to turbulence. Wang et al. (2020) attempted to replicate the seasonality found in tide gauges in the Bohai Sea using a three-dimensional MITgcm model based on Müller's study with limited results. Ray (2022) proposes several physical mechanisms underlying the seasonality of the M2 tide group: climate-induced variations such as those found by Müller et al. (2014), astronomical changes due to the Sun's third-body perturbations of the lunar orbit, which are small, and compound tides such as the MSK2 tide. Ray (2022) used long-duration O(10 yrs) data sets taken from St. Malo (France), Chittagong (Bangladesh), and Port Orford (Oregon), which allowed the high-resolution spectral analysis necessary for such a study. Our study cannot capture the small frequency differences in the M2 tidal group, and we shall refer to them as the same constituent.

Drifters in the Eastern Levantine basin have also been used to study the tides in the region (Poulain et al., 2018). There are spatial and temporal limitations to using drifters for tidal analysis. Temporal constraints apply to the sampling frequency and period following signal analysis theory. More broadly, the confidence interval of the estimated values becomes narrower as the period increases (Bendat & Piersol, 1971). This phenomenon is experimentally shown in Lie et al. (2002), where longer, drifter datasets resulted in less deviation from the known M2 and K1 harmonic constants in the Yellow Sea. As for spatial limitations, when a drifter is transported hundreds of kilometers meridionally, the inertial frequency it experiences can vary significantly. As stated above, the inertial period is near the diurnal frequencies in the Eastern Mediterranean (specifically at DeepLev). Work on the M2 tide by Carrère et al. (2004) shows the M2's amplitude is not stable in areas where ocean mesoscale activities occur as well as areas with strong topographic features. The topography near the Israeli coast can change vastly, further affecting the tide, as seen in Rosentraub and Brenner (2007) through multiple moored devices along the coast. For these reasons, a maximal length of a dataset of the spatial order of 1°x1° is needed to minimize the variability of the results due to spatial changes while keeping an accurate tidal harmonic analysis and spectral analysis.

144 Our results from pressure observations near the Israeli coast demonstrate a dominant M2
145 tide constituent presence in every season and at all depths. In the current measurements, tidal
146 analysis shows weak semi-diurnal and diurnal tides at all depths, with a seasonal difference
147 between 3 cm/s in the fall and 0.9 cm/s in the spring for the tidal constituent of K1 at 30 m. In
148 general, seasonality variations are less pronounced with depth. We also compared the tidal
149 constituents' magnitudes derived from surface drifters to those derived from moored instruments.
150 We demonstrated the difficulties associated with balancing the temporal length of the drifter's
151 trajectory and its meridional movement.

152

153 The paper's order is as follows: Section 2 describes the data used and analysis methods.
154 In section 3, we present our results and conclude in section 4.

2 Data and Methods

The currents and pressure were measured at DeepLev (Fig. 1) ~50 km offshore Haifa, Israel, (33◦ 03.67' N; 34◦ 29.296' E), where the water depth is ~1500 m (Katz et al., 2020). The instruments were deployed for 6-9 months, with gaps in the data between consecutive deployments and occasionally within the deployment periods. For simplicity, we converted pressure from decibar to m using a 1:1 ratio for all the analyses presented in this paper. Table S1 provides details on the analyzed time segments.

Currents were measured using Acoustic Doppler Current Profilers (ADCPS) employed at various depths. Three downward-looking Teledyne RDI ADCPs: One 300-kHz system was situated at approximately 30 m depth and measured from 30 m to 100 m in a 2 m bin, and formed ensembles every 15 min; A 150-kHz system was deployed at approximately 100 m, with 4 m bin size, formed an ensemble every 1 hr, down to about 200 m depth; Another 150-kHz system was at approximately 400 m and measured currents in 400-675 m, at 10 m bins and created ensembles every two h. Two Nortek Aquadopp single-point current meters were fixed at depths of 1310 m and 1492 m, measuring temperature, pressure, and currents, creating ensembles every ½ h. Five discrete depths were chosen from the measurements to analyze the current at different depths: 30 m, 50 m, 70 m, 160 m, 400 m, and 1300 m. These observed currents were used before to study intraseasonal variability (Feliks et al., 2022); here, we use the data to study the tides.

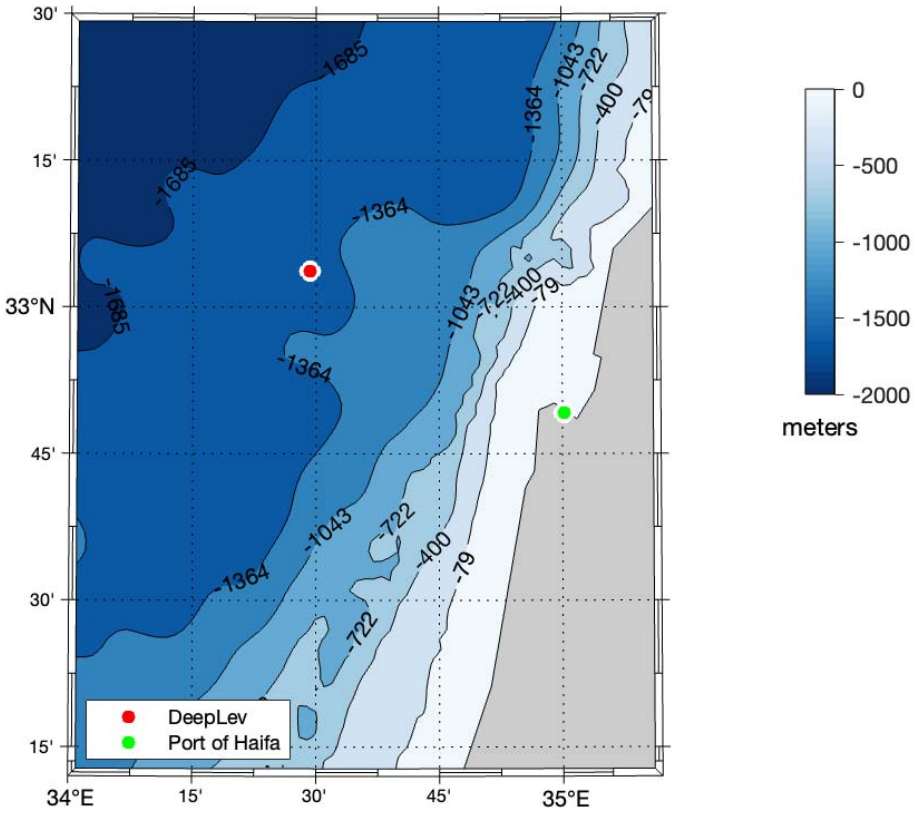

Figure 1. The location of the DeepLev mooring station (white full circle with a red dot), the location of the Port of Haifa (white circle with a red dot), with bathymetry contour color.

Pressure variability was recorded by two RBR-CONCERTO CTDs placed at 80 m and 290 m depths, measuring at a time resolution of 10 min in the first deployment and one min in the following deployments. A SeaBird MicroCat CTD, placed at 185 m, was added to the array starting deployment two with a time resolution of 10 min throughout. CTD depths are noted as 80 m, 200 m, and 300 m. Additional pressure measurements were used from the Nortek Aquadopp at 1310 m, noted as 1300 m.

To analyze the M2 and S2 tides, which have a difference of 0.0028 cycles per hour, a minimum of 15-day hourly data is required to separate the frequencies in a spectral analysis based on the Rayleigh criterion $\Delta f=1/T$ using an unsmoothed periodogram or a rectangular window. For smoothed periodograms or other windows, such as the ones used here, even longer data sets are required (for more details regarding the Rayleigh criterion, see Thomson & Emery (2014)). However, the criterion will produce peaks that are "just resolved"; this period length is not long enough to ensure no leakage between the two frequencies. "Well-resolved" peaks have a criterion $\Delta f>3/2T$ for unsmoothed periodograms. Here, we compare the common 15-day data

length set with longer data sets of 22.15-day (hereafter referred to as 22-day) or 30-day to evaluate the impact of spectral leakage on instrumental data.

The comparison is made in Section 3.2.2 using data from the first 60 days of the four seasons from 2017. Only 60 days were taken in the analysis since there are gaps between deployments in 2017, giving two seasons with less than 90 days to compare the 15-day, 22-day, and 30-day analyses. For the 15-day analysis, a season was split by taking the first four 15-day segments with no overlap. After the tidal harmonic analysis, the magnitudes were averaged to give one result for the 15-day segment. For the 22-day analysis, the same season was split into the first three 22-day segments with no overlap. After the tidal harmonic analysis, the magnitudes were averaged to give one result for the 22-day segment. For the 30-day analysis, the same season was split into the first two 30-day segments with no overlap. After the tidal harmonic analysis, the magnitudes were averaged to give one result for the 30-day segment. All analyses were done for three different depths of 70 m, 160 m, and 1300 m.

Section 3.3 also used the trajectories of surface drifters deployed along the Israeli coast. The drifters used were the Surface Velocity Programme SVP drifter design with a drogue centered at 15 m depth, manufactured by METOCEAN. Each drifter provides its location through the global positioning system (GPS) and transmits the data on land via the Iridium satellite link. The drifter position time series were first edited from spike and outliers, then linearly interpolated at regular 0.5-h intervals using the kriging technique (optimal interpolation; Hansen & Poulain, 1996). Velocity components were then estimated from centered finite differences of 0.5-h sub-sampled positions (Menna et al., 2018).

We analyzed periods of 15-day with 50% overlap, 22-day with 50% overlap, and 30-day with 50% overlap where drifters were within 1° of DeepLev. The locations of the drifters (in Latitude-Longitude coordinates) were converted to velocities using a first central difference algorithm from the MATLAB package by Lilly (2021). We split the drifter data into segments of 15, 22, and 30-day to study the M2 and S2 tides. The current data from DeepLev, analyzed in section 3.3 as a comparison with drifter data, was taken from 50 m depth due to the lack of continuous data at shallower depths for most of the drifters' deployments. Only during the first deployment was their data at around 10 m. Matlab's corr function calculated the correlation coefficient between the 10 m, 30 m, and 50 m u (eastward velocity) and v (northward velocity) data above 0.89 with a p-value of practically null.

The choice of the bin size of 1° from DeepLev is based on the work done by Carrère et al. (2014) on the global stability of the M2 tide. Focusing on semidiurnal tides arises from the "contamination" by near-inertial oscillations and diurnal breeze (Poulain et al., 2018) on the diurnal tides. There were 32 segments of 15-day from 14 different drifters covering the seasons of 2017 and the summer of 2018. Of these segments, four were in the winter, 10 in the spring, 15

in the summer, and three in the fall. There were 12 segments of 22-day from 5 drifters. Of these segments, one was in the winter, six in the spring, four in the summer, and one in the fall. There were seven segments of 30-day from 3 drifters covering the spring and summer of 2017 and one remaining in the spring of 2018.

Tidal harmonic analysis was done using the t_tide MATLAB package (Pawlowicz & Lentz, 2002). The magnitude of the current signal was computed by taking the square root of the amplitudes of semi-major and semi-minor axes. Amplitudes and corresponding Signal-to-noise (SNR) were estimated using a linearized error analysis that assumes a red noise model (Pawlowicz & Lentz, 2002). All tidal constituents' amplitude and inclination following will be those found to have an SNR of above 1. Hereinafter, we will refer to the magnitudes of the current signal as magnitude and the amplitudes of the pressure variability signal as amplitudes. The average magnitudes and amplitudes were calculated only concerning results with an SNR above 1; the rest were labeled Not Significant (N/S). The toolbox gives the explained variance of the significant tidal signal.

We also conducted spectral analysis (Power Spectral Density, PSD) using a multitaper method introduced by Thomson (1982) and further utilized in a MATLAB package by Lilly (2021). In this analysis, the PSD graphs are rotary spectra of the currents and the real-valued time series for the pressure. Four Slepian tapers were used for the rotary spectra, while for the pressure, one Slepian taper was used (Slepian, 1978). Significance levels of 95% were calculated using the signal's red noise spectra as the null hypothesis and F-test statistics to find the 95% significance levels. The degrees of freedom (DOF) are calculated $K = 2P-1$ where K is the DOF, and P is the number of Slepian tapers used in the analysis. We used this assuming that singly tapered spectral estimates follow a scaled chi-squared ($\chi 2$) distribution (Percival & Walden, 1998).

All the samples have been split by season, defined as winter (December-February); spring (March-May); summer (June-August); and autumn (September-November). A description of the exact durations is presented in Table S1. Due to the nature of the study into diurnal and semidiurnal tidal constituents, a required resolution of 0.001 cycles per hour is needed to differentiate between the tides, detailed in Table 1, and various tidal constituents in their spectral vicinity. This limitation excludes any sample shorter than 30 days, except for the drifter analysis. Segments were also cut by a restriction of a maximal gap of 3 hours between credible data points (credible as defined by Katz et al., 2020). If a segment has two parts with a gap larger than 3 hours in between, the longer segment was used to represent the season. For gaps shorter than 3 hours, a linear interpolation was used. After interpolation, a linear detrend was performed.

The 400 m depth data is sampled every 2 hours, and this sampling cannot use the linearized error analysis offered by the T_Tide library, which requires a maximum delta of 1 hour. For this data set, we used a white random noise error analysis offered by the T_Tide library, which has a

slightly less conservative SNR than the linearized error analysis. Even with this difference, the analyzed data from the 400 m data set did not differ substantially from the other analyzed data sets. To further compare our results from DeepLev, we used the OSU TPXO model (Egbert & Erofeeva, 2002) positioned at the location of DeepLev (33◦ 03.67' N; 34◦ 29.296' E).

Tide	Period
Primary tides of the study	
S2	12 hr
M2	12.4 hr
K1	23.9 hr
O1	25.8 hr
Other tides mentioned in the study	
UPS1	21.5 hr
Mf	13.66-day
Msf	14.8-day

Table 1. Tidal constituents and their periods are either the primary focus or are mentioned in this paper.

3 Results

3.1 Pressure Variability

CTDs at depths of around 90 m, 200 m, 300 m, and 1300 m recorded pressure during six deployment periods between 11/2016 and 11/ 2020. Except during winter, most records show a 1-2 m variability. The winters show a much higher variability, reaching levels over 20 m, as seen in Jan 2019 (Fig. 2).

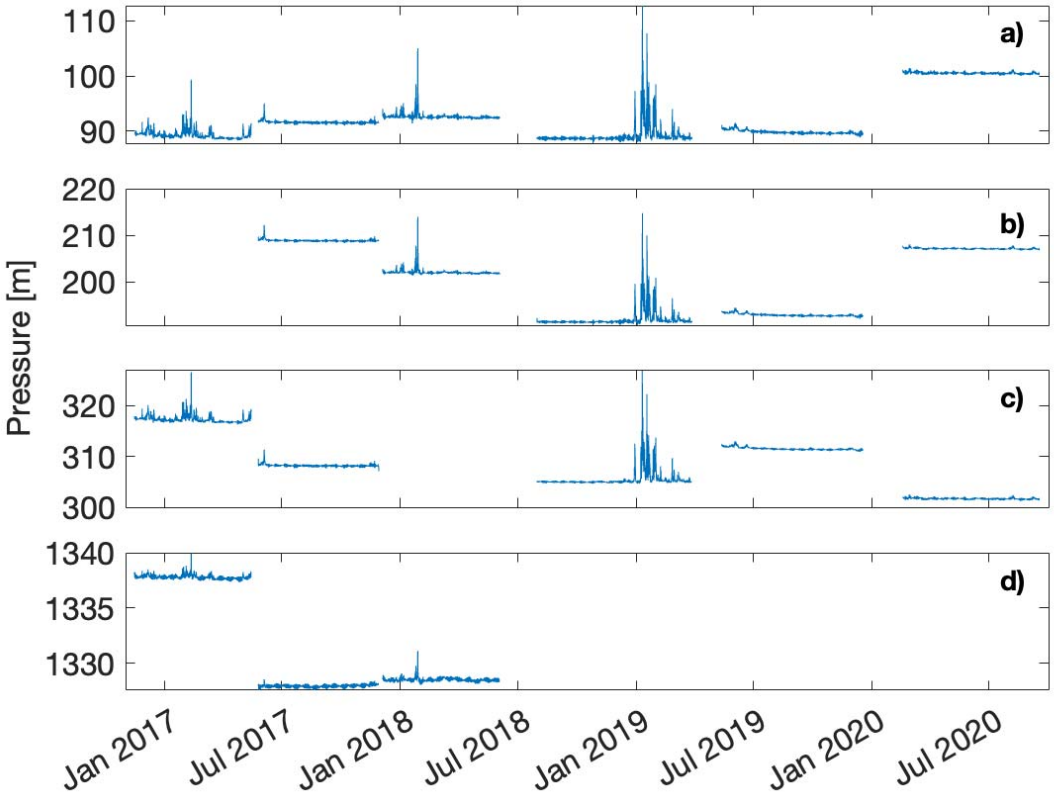

Figure 2. Pressure time series, measured in m, at four depths measured: (a) 90 m, (b) 200 m, (c) 300 m, and (d) 1300 m. Measurements started in November 2016 and ended in June 2020. There were no measurements for all the depths, as described in Table S1. Each deployment was measured at a slightly different depth, which is the reason for the differences in pressure between deployment periods.

The large fluctuations in the winter, specifically in Jan 2019, might be due to a tilting of the mooring device from strong horizontal motions (Katz et al., 2020). The currents could result from a mesoscale eddy passing in the area of DeepLev. As shown in Feliks and Itzikowitz (1987), the characteristics of eddies in the Eastern Mediterranean can bring changes and displacements in temperature and pressure of around 20 m at depths down to 300 m. A study of the temperature changes, shown in Fig. 3 around January 2019, shows similar results to those that characterize an eddy in the Eastern Mediterranean. Synoptic maps (not shown) of pressure from NCEP reanalysis in January do not display any storm in the area. In general, along with the tides, strong horizontal currents may tilt the mooring devices, creating motions that may be interpreted as vertical perturbations. To move the devices vertically 22 m, the approximate maximum vertical variation in Fig. 3, the tilt needed is approximately 10.5 degrees, giving a horizontal deviation of 236.9 m.

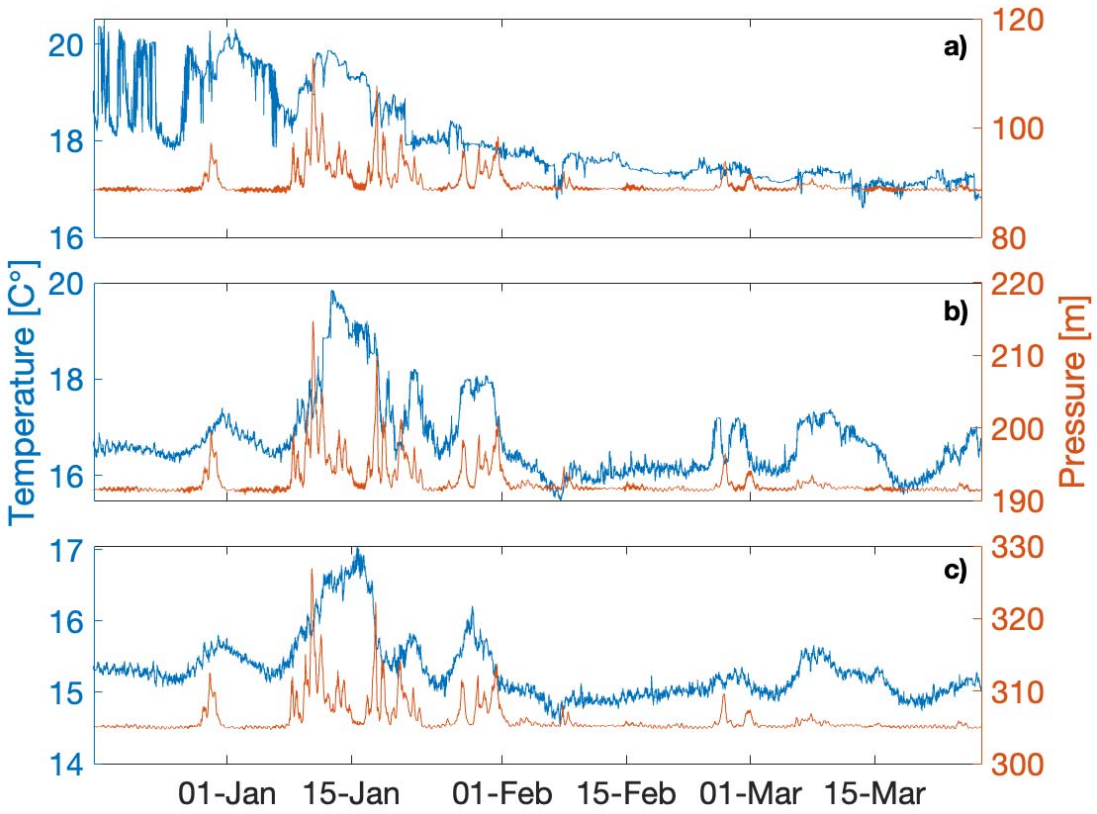

Figure 3. Temperature and pressure time series, measured in degrees Celsius and m, at three depths measured: (a) 90 m, (b) 200 m, and (c) 300 m between 17/12/18 and 27/3/19.

3.1.1 Tidal Analysis of Pressure Variability

Several tidal constituents are evident in the pressure variability. The foremost semidiurnal and diurnal tides, S2, M2, K1, and O1, vary slightly between years and depths (Table S2 in the appendix), demonstrating the barotropic characteristics. This agrees with several models calibrated with experimental results (Tsimplis et al., 1995; Arabelos et al., 2011) and a time series in the Western Mediterranean (Alberola et al., 1995).

The amplitude of M2 is the most dominant. It varies with time and depth between 9.5-12 cm, in good agreement with tide gauges (Tsimplis et al., 1995), models (Tsimplis et al., 1995; Arabelos et al., 2011) as well as the OSU TPXO barotropic model (Egbert & Erofeeva, 2002) with an amplitude of 10.7 cm. The M2 amplitude is consistent, with no evident seasonal or depth variability. The S2 amplitude ranges between 5.6-8.3 cm, with no depth variability but with seasonal variability, as seen in Fig. 4, with fall averaging 8.2 cm and summer averaging 6.1 cm. The results from previous studies (Tsimplis et al., 1995; Arabelos et al., 2011) show a range of 7-8 cm, and the OSU TPXO shows 6.2 cm. O1 ranges between 2-3 cm, with few singular exceptional amplitudes of 10 cm found in all depths of winter 2017, larger than the previously

observed and modeled results of 1-2 cm and the OSU TPXO showing 1.9 cm. The K1 tide varies with season, with larger amplitudes in winter (~10 cm) at 90 m depth and summer amplitudes in the 2.5-3.5 cm range. The significant differences between seasons in K1 are smaller at 1300 m with amplitudes of 3.5-4 cm in the winter and 2.5-3 cm in the summer. These results are also larger than predicted or recorded in previous studies of 1-2 cm, and the OSU TPXO shows 1.7 cm. The changes in depth can be attributed to the leakage of atmospheric stress to the diurnal bands. The O1 and K1 are anomalously high in the winter, significantly larger than previously observed. A possible explanation for the heightened amplitude is the leakage of the inertial period into the diurnal frequencies due to winter eddies near DeepLev, such as the one showcased in section 3.1.

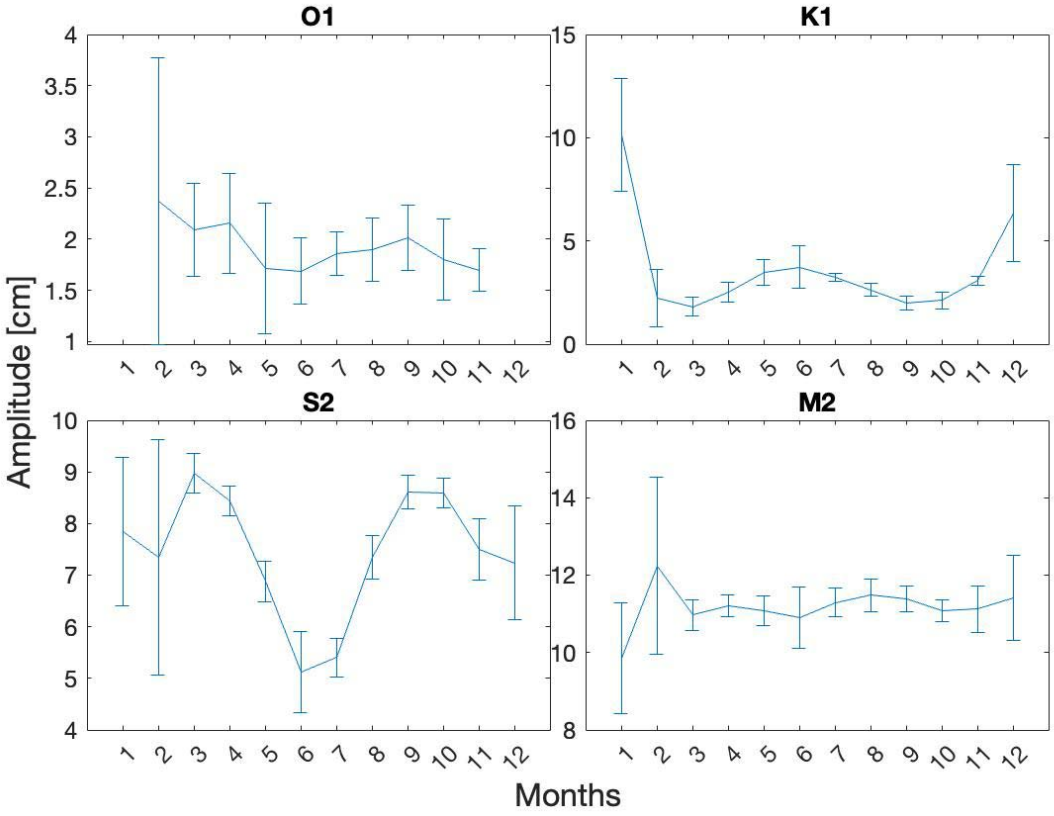

Figure 4. The average monthly amplitudes [cm] of the four major tides analyzed from the 2017-2020 pressure time series at 200 m depth. The vertical lines are average error bars retrieved from the harmonic analysis. The seasonal trends for all the tides are the same at 90 m and 300 m depths.

A fortnightly oscillation is present only in the summers at all depths, as seen in Table S2, as well as in the raw pressure data (Fig. 5). At the same time, it is not found significant in the spectral analysis shown in Fig. 6. This might be explained by non-linear interactions between semidiurnal and diurnal tides which have been argued to amplify the oscillations (Kwong et al., 1997). In Fig.

5, a reconstruction of only the M2 and S2 tides shows the spring and neap tides, similar to the fortnightly oscillations observed in the raw data emphasized in the bottom graph.

Another significant tide identified was the UPS1 tide (Table S2). The amplitude range is wide from 0.5-10 cm at 90 m with no apparent pattern regarding changes between seasons apart from winter months, where the largest amplitudes were found. The UPS1 oscillation is less considerable in the pressure analysis than in the currents detailed in section 3.2.1. The UPS1 tide has been observed in sea level variability analysis in Alexandria (El-Geziry & Radwan, 2012; El-Geziry 2021; Khedr et al., 2018) with amplitudes below 1.5 cm. These results were taken from tide gauges along the Port of Alexandria. However, the UPS1 tide found can possibly be attributed to near-inertial internal waves due to the clockwise motion of the current measurements when the UPS1 tide is present (not shown). Motions in the near-inertial regime can generate near-internal waves that do not only oscillate in a purely horizontal plane, such as inertial oscillations, but also vertically, albeit with much smaller vertical amplitudes than internal tides (Alford et al., 2016). The amplitude of this tidal constituent declines with depth over all seasons, which is also consistent with near-inertial oscillations.

Tidal constituents represent a significant portion of the variance of the pressure time series for most of the year. The variance variation in 2017 regarding season and depth is demonstrated in Table 2. Before analyzing the trends in the table, it is important to note a few anomalies of 2017 from the other years used in this research. The variance in the spring is unusually high, with the variance in 2018 and 2020 at $1.1*10^{-2}$ for all depths apart from 1300, for which we do not have further data. Furthermore, summer and fall percentages are uncharacteristically small, with summer percentages starting around 40% and fall percentages around 70%. With that, the general trends found in Table 2 are relevant and similar for all the years in the study.

With depth, for all the seasons except fall, we see a slight drop in tidal variance for the top 300 meters and a decline to what appears to be a baseline variance of approximately $1.1*10^{-2}$ m at 1300 m. The opposite can be said for the role of the tides in the total variance, which increases with depth due to the waning effects of atmospheric forces with depth. At 1300 m, seasonal changes of tidal variance are negligible, while for the percentages, we see that seasonal changes continue to appear in the deep. With seasonality, at the top 300 m, the variance and percentages vary from the baseline variance in winter and summer in all the years of the dataset, except spring 2017. Winter is found to have the greatest variance, then summer with a smaller variance. Fall is the season with the highest percentage of tidal variance from the total variance, then summer and spring with roughly similar numbers, and winter with the least tidal variance from the total variance.

	Winter	Spring	Summer	Fall
90m	$2.5*10^{-2}$ **(2.7%)**	$4.7*10^{-2}$ **(19.9%)**	$1.8*10^{-2}$ **(24.2%)**	$1.1*10^{-2}$ **(49.3%)**
200m	-	-	$1.8*10^{-2}$ **(25.1%)**	$1.1*10^{-2}$ **(52.2%)**
300m	$2.2*10^{-2}$ **(2.9%)**	$4.2*10^{-2}$ **(20.4%)**	$1.7*10^{-2}$ **(25.8%)**	$1.1*10^{-2}$ **(54.1%)**
1300m	$1.1*10^{-2}$ **(20.6%)**	$1.1*10^{-2}$ **(41.4%)**	$1*10^{-2}$ **(77.2%)**	$1.1*10^{-2}$ **(84%)**

Table 2. Total tidal variance in m and the percentage of the tidal variance (in bold) from the total variance of the pressure time series found per season of 2017 and at four depths. Only tidal constituents with an SNR of above one are considered in the tidal variance.

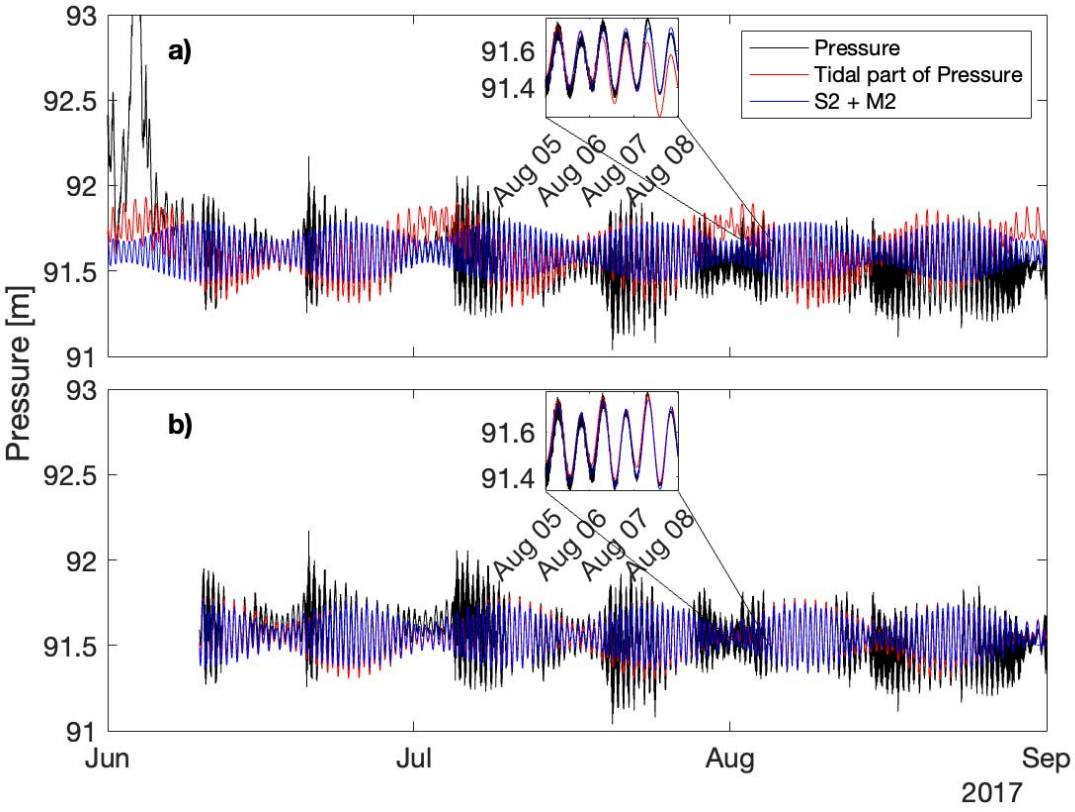

Figure 5. A sample of the pressure time series in m at 90 m from summer 2017 where the top graph includes a sudden pressure jump in the analysis and the bottom graph the pressure jump is excluded from the analysis. Both graphs include the raw time series (black), the reconstruction of the amplitudes of all the significant tides of the season (red), and the reconstruction of only the S2 and M2 (blue). In the inset, there is a zoom-in on a three-day interval in August. It is clear from both graphs the importance of the significant tides, and specifically the semidiurnal tides, on the pressure. From the zoom-in of both graphs, we can see that the pressure jump distorts the

harmonic analysis, where the total reconstruction (red) behaves differently between the two graphs.

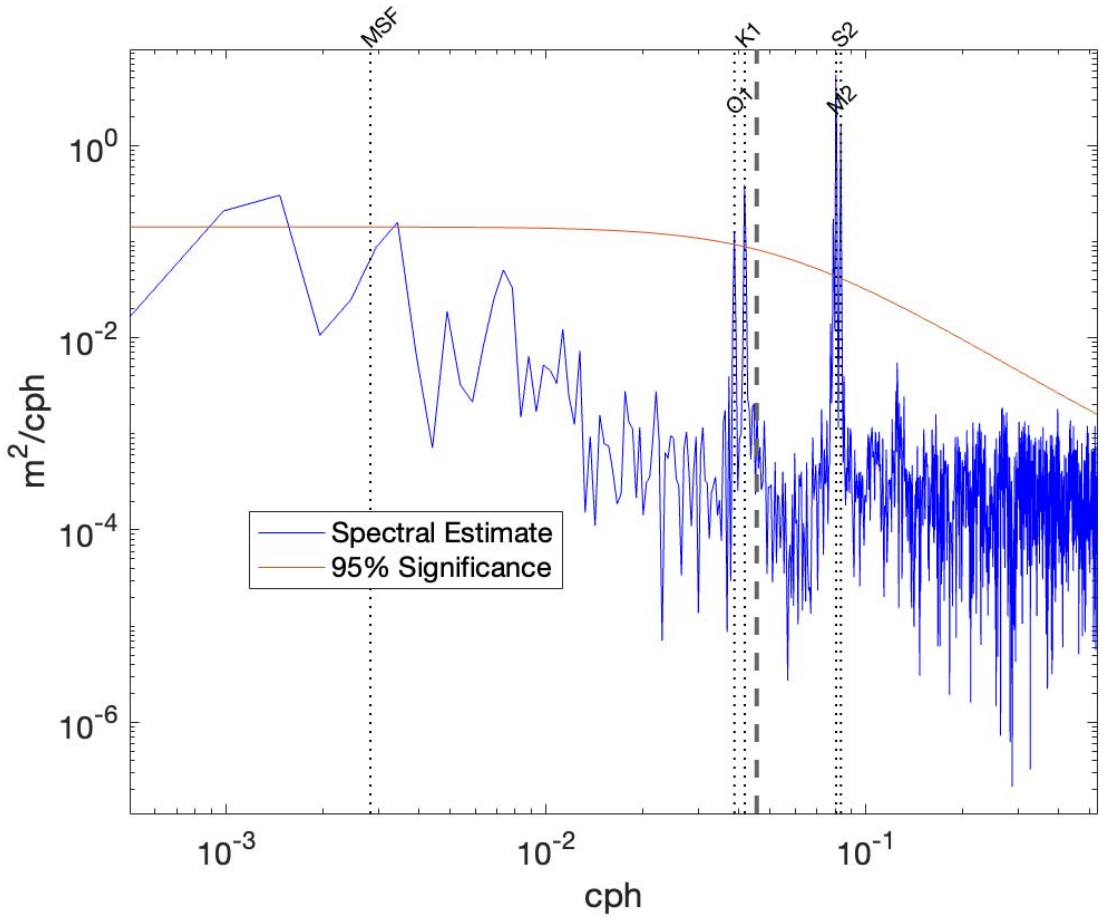

Figure 6. The Power Spectral Density in m^2/cph of the pressure time series as a function of cph (log-log) at 300 m depth in the summer of 2017. The dashed vertical lines in the graph indicate tide constituents; Msf, O1, K1, M2, and S2. The red curve indicates the 95% Significance Level with respect to red noise. The diurnal and semidiurnal amplitudes are significant in the spectrum. The MSF fortnightly oscillation peak is seen to be insignificant in the spectral analysis as opposed to the tidal harmonic analysis.

3.2 Current Variability

The currents were dominated by episodes of strong flows, particularly in the winter, as seen in Table 3 and Fig. 7 and 8.

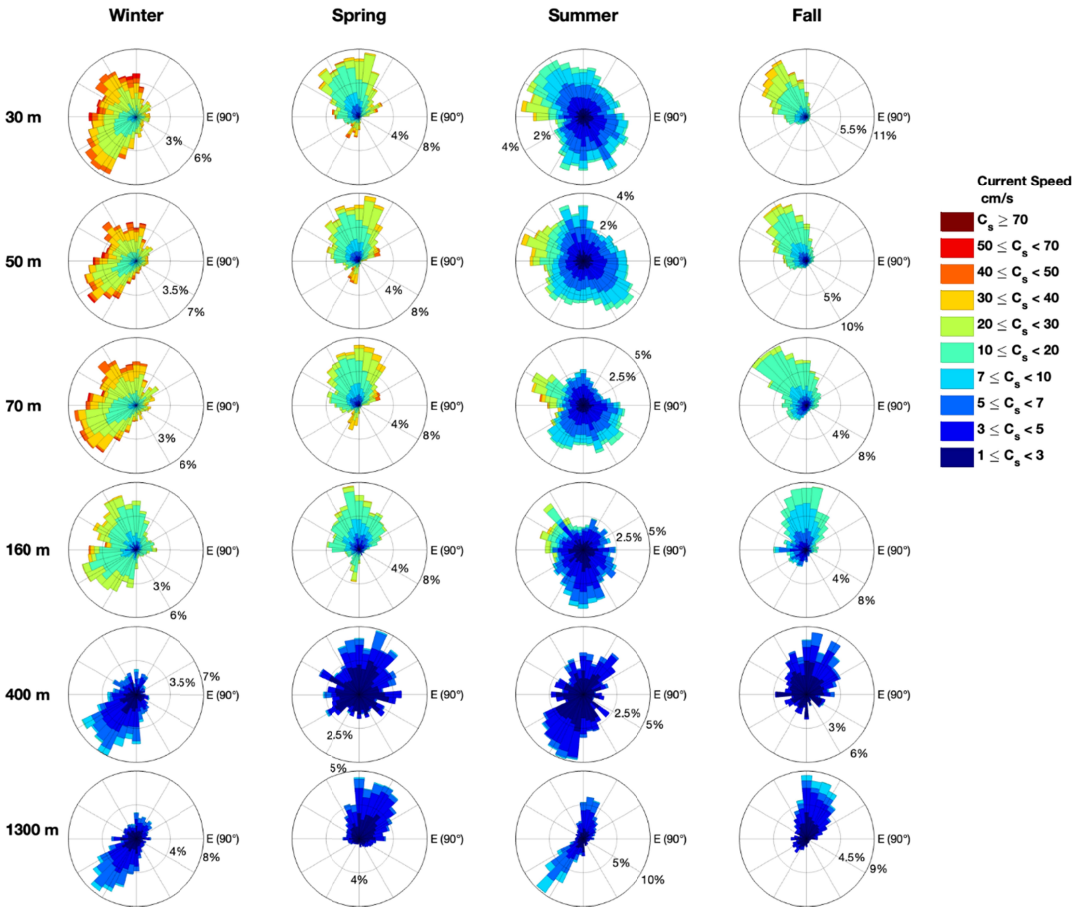

Figure 7. Current rose of the currents at the depths of 30 m, 50 m, 70 m, 160 m, 400 m, and 1300 m during the winter, spring, summer, and fall periods of 2017. The units of the current rose are in cm/s. Each record of a given current in a times series is projected in its direction and added to a bin matching the ranges in the legend. The larger the bin size, the more frequently the speed counted in that direction. The approximate frequencies of occurrence can be seen by the percentages shown.

	Maximum recorded speed	Date of max recorded speed	Winter mean speed	Spring mean speed	Summer mean speed	Fall mean speed
30m	78.4	30-Dec-18 15:45:00	20.5	14.1	9	12.6
50m	74.4	30-Dec-18 05:15:00	20.4	14.1	9	10.7
70m	68.8	10-Jan-19 16:30:00	19.2	13.8	8.7	8.7
160m	43.2	10-Feb-17 19:00:00	11.3	9.2	5.8	5.4
400m	19.9	13-Jan-19 00:00:00	4	3	2.7	2.4
1300m	12.2	06-Jan-18 12:00:00	2.3	2	1.2	1

Table 3. Maximum recorded speeds (magnitude of the horizontal currents) at different depths (cm/s) were found in all the years of the dataset (cm/s) and the dates they were found. Season mean results are the season average from the three years of observations.

In Table 3, a weakening in speed with depth is evident, and a smaller dependency of the seasons on the speed at 1300 m. The flow across the entire water column is mainly meridional (roughly parallel to isobath); an example is shown in the feather diagram in Fig. 8.

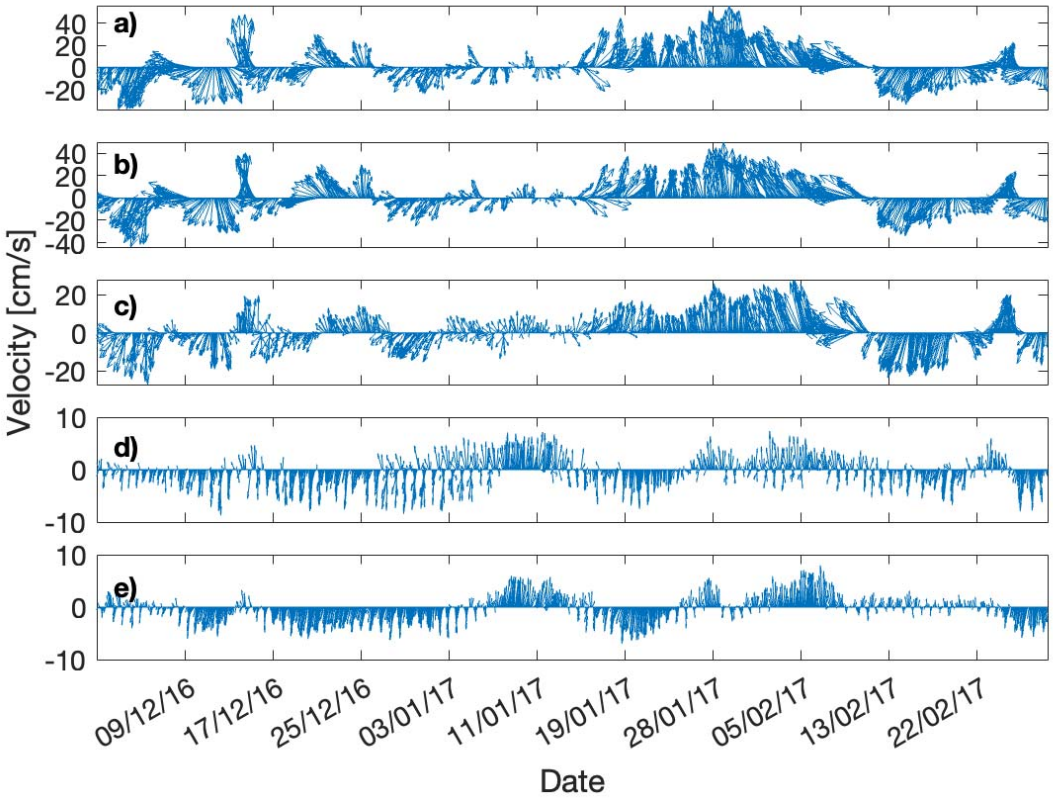

Figure 8. A feather diagram showing the currents (cm/s) during winter 2017. Each subplot depicts a different depth, in ascending order of 30 m, 70 m, 160 m, 400 m, and 1300 m. The velocities of 30 m, 70 m, 160 m, and 1300 m depths were averaged for a two-hour sampling period. Note the different scales for the different depths.

A dominant flow direction at the near-surface is toward the north in the spring. At the same time, an almost sporadic motion occurs in the summer (Fig. 7). The continental shelf break is parallel to the coast (Fig. 1), and in the fall, the near-surface currents move perpendicularly away from the shelf. The winter also shows movement away from the shelf but no specific direction. At 1300 m depth, the directions of currents are split between northwest, along the shelf break, during spring and fall, and southeast during the summer and winter.

3.2.1 **Tidal Harmonic Analysis of Current Variability**

For the four main tidal constituents of the study, O1, K1, M2, and S2, different results arise from the current analysis than from the pressure analysis. The UPS1 is the single most prominent tide in the tidal harmonic analysis done on the currents, yet it can be attributed to the near-inertial band and will not be discussed further in the results.

The S2 and M2 are significant sporadically near the surface, with nearly negligible magnitudes of roughly 0.3 cm/s for the S2 and between 0.3-0.6 cm/s for the M2, as seen in Table S3. For the M2, this is an order of magnitude weaker than the drifter data found in Poulain et al. (2018). Still, for the S2, the results are consistent with Poulain et al. (2018) findings, which show currents between 0-1 cm/s, while the results from the drifter data are generally larger for both the 15-day (0.6-3 cm/s) and 30-day (0.7-1.3 cm/s) analysis. The OSU TPXO model finds a semi-major ellipse axis for the M2 current of 9.7 cm/s and 5.8 cm/s for the S2 tidal current, with values larger than those in this study. At 1300 m, the S2 and M2 are significant across the seasons, with magnitudes of 0.1-0.2 cm/s for M2 and 0.1-0.2 cm/s for the S2 tide (Table S3).

An opposite trend occurs for the diurnal tides. At 30 m, the K1 (Table S3) tidal constituent is significant across all seasons, ranging from 0.9-3 cm/s. Seasonal variability is present, with fall being the strongest season and summer-spring the weakest tidal currents. With depth, K1 starts to be less significant until 1300 m, where the constituent is not significant across all seasons. This might be due to intense wind stress originating from the daily breeze, as suggested by Alvarez et al. (2003), Poulain et al. (2018), and others. The O1 tidal currents are also less significant with depth, as seen in Table S3, with a range of velocities between 0.9-1.9 cm/s at all depths. In most segments, the analysis did not find significant oscillations of the O1 tide.

The variance of the significant tidal constituents plays a minor part in the overall current variance, depicted in Table 4. Feliks et al. (2022) showed that the intraseasonal oscillations are generally larger (above 4 cm/s) than the tides in the Eastern Mediterranean shown here. The results which are inconsistent with the other years are the weak top 160 m in the winter, which are typically above 10 cm/s and have a much higher percentage of variance, and the large variance found in the fall at 70 m with a smaller than usual percentage for the top 50 m in the same season. At 1300 m in fall, there is a very low tidal variance, yet we can not with confidence that this is out of the ordinary since we do not have any more data about the fall season of a different year.

The general trends in 2017, shown in Table 4 and the rest of the analyzed data, show stronger tidal currents in the winter and spring, with a slump in summer. As in the pressure analysis, tidal variance lessens with depth, yet the percentage of tidal variance from total variance grows with depth. Unlike with the pressure analysis, it doesn’t seem like there is a baseline variance.

	Winter	Spring	Summer	Fall
30m	-	35.9 **(16.5%)**	5.4 **(18.4%)**	6.9 **(4.7%)**
50m	3.4 **(0.6%)**	37.3 **(17%)**	8.2 **(13.2%)**	4.4 **(4.7%)**
70m	3.2 **(0.6%)**	34.7 **(16.7%)**	8.2 **(13.5%)**	19.43 **(30.4%)**
160m	2.8 **(1.2%)**	13.7 **(14.2%)**	4.2 **(11%)**	5.9 **(17%)**
400m	2.8 **(18.3%)**	1.5 **(21.8%)**	2 **(35.2%)**	2.5 **(36.7%)**
1300m	2.8 **(22.1%)**	1.6 **(20.9%)**	1.6 **(10.1%)**	0.1 **(1.2%)**

Table 4. Total tidal variance in cm/s and the percentage of the tidal variance (in bold) from the total variance of the current time series found per season of 2017 and at four depths. Total tidal variance is taken from the T_Tide package as the summation of the total tidal variance of u and v. Only tidal constituents with an SNR above 1 are considered in the tidal variance.

3.2.2 Sensitivity to Dataset Lengths

The data of four seasons from 2017 from DeepLev is analyzed using tidal harmonic analysis in different dataset lengths of 15-day, 22-day, and 30-day, at three different depths of 70 m, 160 m, and 1300 m.

At 70 m depth, on average across all seasons, the M2 tide magnitude from a 15-day analysis is approximately 1.3 times larger than the 22-day analysis and 1.6 times larger than the 30-day analysis. For the S2 tide magnitude, a 15-day analysis is approximately 1.1 times larger than a 22-day analysis and 1.4 times larger than a 30-day analysis. The 22-day period is larger than the 30-day, for the M2 magnitude, by only 1.2; for the S2, it is 1.4 times larger.

At 160 m depth, on average across all seasons, the M2 tide magnitude from a 15-day analysis is approximately 1.3 times larger than the 22-day analysis and 1.9 times larger than the 30-day analysis. For the S2 tide magnitude, a 15-day analysis is approximately 1.5 times larger than a 22-day analysis and 1.8 times larger than a 30-day analysis. The 22-day period is larger than the 30-day, for the M2 magnitude, by 1.4; for the S2, it is 1.5 times larger.

499

500 At 1300 m depth, on average across all seasons, the M2 tide magnitude from a 15-day analysis is
501 approximately 1.2 times larger than the 22-day analysis and 1.1 times larger than the 30-day
502 analysis. For the S2 tide magnitude, a 15-day analysis is 0.9 times larger than the 22-day analysis
503 (this may be due to a lack of significant tides across the seasons, as shown in Table S4) and 1.3
504 times larger than the 30-day analysis. The 22-day period is the same as the 30-day for the M2
505 magnitude, while for the S2, it is 1.4 times larger.

506

507 These results are consistent with the leakage effects of two close frequencies analyzed at exactly
508 their Rayleigh criterion and not their "well-resolved" criterion. In summary, the 15-day analysis
509 for the M2 and S2 results is larger in magnitude than the 22-day analysis, which is larger than the
510 30-day analysis. Appendix D-1 contains a table with the results from the tidal harmonic analysis
511 of the mooring results.

512

513 **3.3 Tidal Harmonic Analysis Based on Drifter Data vs. Moored Instruments**

514

515 Drifter data has been used to estimate harmonic tidal constituents, both globally (Poulain 2015)
516 and regionally (Poulain 2018; Lie et al., 2002; Ohshima et al., 2002) or to compare with tidal
517 prediction models (Zaron & Elipot 2021; Kodaira 2016; Zaron & Ray 2017; Crawford et al.,
518 1998;). Using drifters for tidal current analysis has the benefit of inexpensive observations with
519 short sampling intervals at a distance from the coast, where most of the moored devices are
520 stationed. Lie et al. (2002) demonstrated this in the Yellow Sea.

521

522 In the following tidal analysis, we tested the sensitivity of the semidiurnal tidal constituent
523 results from a tidal analysis done on drifters using different dataset lengths. The results were also
524 compared with current data from DeepLev. The Rayleigh criterion for the S2 and M2
525 constituents is approximately 15 days, yet the stricter "well-defined" criterion is approximately
526 22 days. We used 15, 22, and 30-day datasets for our comparative analysis. We only took drifter
527 trajectories within 1° of DeepLev to limit the spatial variations in tidal regimes.

528

529 **3.3.1 Tidal Harmonic Analysis of Drifter Data from 15-Day Segments**

530

531 Complete details of the drifter data following a tidal harmonic analysis can be found in Appendix
532 D-2. For many segments fitting the predefined criteria, the dominant tide was the S2 tide, as seen

533 in Table 5. Interestingly, the S2 results show a decrease in the magnitude of the tide with the
534 coming of summer, agreeing with the results shown in section 3.2.

535

536 As a comparison with the drifters, a tidal harmonic analysis was done on data from DeepLev
537 from the same dates at 50 m depth, which did not show an explicit dominant tidal constituent and
538 generally smaller magnitudes. It is clear from the moored dataset that the semidiurnal tides are
539 almost the same, yet the magnitudes reported in DeepLev are much smaller for the S2 tide while
540 only slightly smaller for the M2. The magnitudes are also larger than those found in section
541 3.2.1, which agrees with signal analysis theory.

542

543 These results agree with the results found by Poulain et al. (2018), which find both the S2 and
544 M2 with a magnitude of under 2 cm/s. A few notes are important to emphasize. First, the
545 averages were calculated without regard to results with an SNR of below 1. Second, the summer
546 results include segments from the summer of 2017 and 2018. Lastly, the S2 and M2 magnitude
547 behavior, i.e., S2 being greater than M2, was found in different drifter types and years.

548

	M2 - Drifters	**M2 - Mooring**	**S2 - Drifters**	**S2 - Mooring**
Winter	1.7	0.9	1.9	0.9
Spring	1.6	0.9	0.7	0.9
Summer	1.5	0.8	0.8	0.7
Fall	2	0.6	1	0.5

549

550 **Table 5.** Seasonal average magnitudes [cm/s] of the M2 and S2 tidal currents from drifters and
551 DeepLev in 15-day segments.

552

553 **3.3.2 Tidal Harmonic Analysis of Drifter Data from 22-Day Segments**

554

555 The results, as seen in Table 6 from the drifters' 22-day segments, were, in general, smaller in
556 magnitude than the results from the 15-day segments, a result that is consistent with theory and
557 seen in section 3.2.2. The dominant S2 seen in the 15-day drifters also subsided and is almost the
558 same as the M2 apart for the summer and fall results, with fall containing only one segment. As
559 for the results from DeepLev, the magnitudes were roughly the same for both the 15 and 22-day
560 segments. It is important to note that by raising the time limit to 22 days, fewer segments were
561 used, with fewer significant results for the tides. Complete details of the relevant drifter segments
562 following a tidal harmonic analysis can be found in Appendix D-3.

563

	M2 - Drifters	**M2 - Mooring**	**S2 - Drifters**	**S2 - Mooring**
Winter	1.1	1	1.2	N/S
Spring	1.4	0.8	1.1	0.6
Summer	0.8	0.8	1.3	0.5
Fall	N/S	N/S	2	N/S

564

565 **Table 6.** Seasonal average magnitudes [cm/s] of the M2 and S2 tidal currents from drifters and
566 DeepLev in 22-day segments. N/S indicates values with a signal-to-noise ratio below 1 in the
567 tidal analysis.

568

569 **3.3.3 Tidal Harmonic Analysis of Drifter Data from 30-Day Segments**

570

571 Only seven drifter segments were found to be 30 days near DeepLev. Full details of the drifter
572 data following a tidal harmonic analysis can be found in Appendix D-4. Unfortunately, there is a
573 gap in the mooring data around when the drifters were in its proximity, so few results can be
574 compared. An example of a drifter's 30-day trajectory can be found in Fig. 9 with what seems
575 like near-inertial oscillations of the drifter.

576

	M2 - Drifters	**M2 - Mooring**	**S2 - Drifters**	**S2 - Mooring**
Winter	N/D	N/D	N/D	N/S
Spring	N/S	0.7	1.2	0.6
Summer	0.8	0.6	0.6	0.5
Fall	N/D	N/D	N/D	N/S

577

578 **Table 7.** Seasonal average magnitudes [cm/s] of the M2 and S2 tidal currents from drifters and
579 DeepLev in 22-day segments. N/S indicates values with a signal-to-noise ratio below 1 in the
580 tidal analysis. N/D indicates areas with no data.

581

582 To summarize the tidal harmonic analysis on different drifter dataset lengths, the results show a
583 weakening of magnitude of the M2 and S2 tide as the dataset grew longer. This was less
584 pronounced in the equivalent mooring dataset, yet the trend remained.

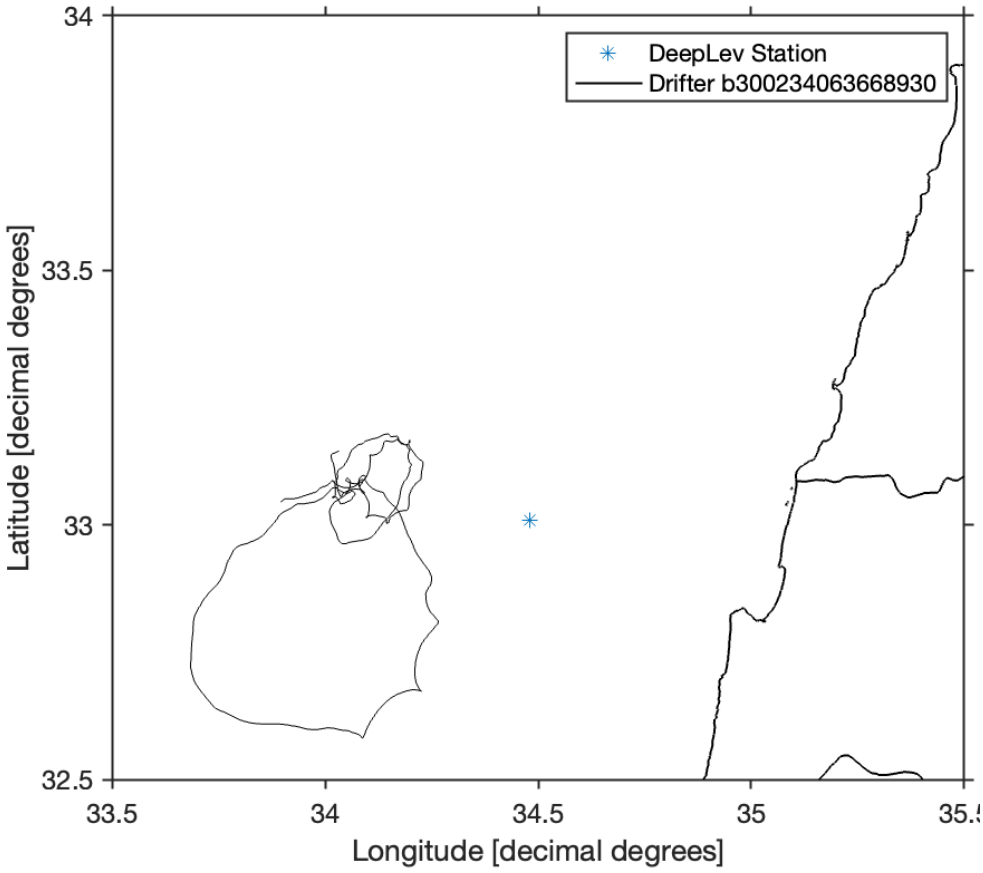

585

586 **Figure 9.** Example of the trajectory of drifter b300234063668930, surrounding DeepLev
587 (marked by a blue star), used to analyze the semidiurnal tidal constituents M2 and S2 between
588 27-Apr-2017 06:00:00 and 27-May-2017 05:00:00.

589

590 **4. Discussion & Conclusions**

591

592 Data from both the moored mooring station and surface drifters in its vicinity were used to study
593 the structure of tides both from currents and pressure in the Eastern Levantine basin at
594 semidiurnal (M2 and S2), diurnal (K1 and O1) and longer (Msf) periods. The pressure variance
595 explained by the tides is substantial at all seasons apart from the winter, with the most significant
596 season being the fall (average of 67% explained variance), increasing in explained variance with
597 depth. Unlike the pressure, the variance of the current explained by the tides is less considerable,
598 with little variation with depth and spring holding the highest portion of tidal explained variance
599 (average of 19%). A much larger variance is explained by intraseasonal variability (Feliks et al.,
600 2022).

601

The M2 was the most dominant frequency with amplitudes similar to both tide gauge and model results (Tsimplis et al., 1995; Arabelos et al., 2011). No variability due to seasonal changes was evident in the M2 amplitude. For the S2, a change in amplitude of 2 cm can be discerned between summer and fall averages. Even with this variability, previous studies and the OSU TPXO model show that this range generally agrees with previous results. As proposed previously, the seasonal variation of tides can result from several reasons. Müller et al. (2014) argued that stronger stratification leads to less loss of energy from the barotropic tide to turbulence and mixing, and Ray (2022) proposed that compound tides with frequencies very near the vicinity of the M2 tide as well as astronomical modulations of the Sun's third-body perturbations of the lunar orbit play a role in the observed seasonality of the M2 tide alongside climate processes.

Sharp variability due to the change of seasons and depths was found in the K1 signal, with amplitudes reaching up to 10 cm in the winter at depths near the surface, significantly higher than previously reported, and down to 2-3 cm in the summer, slightly larger than the models and observations. Although out of the scope of this paper, rudimentary seasonal spectral analysis of coastal wind speed from a meteorological site on the Israeli coast shows strong semidiurnal and diurnal frequencies during the winter as opposed to the rest of the year. Another possible explanation for these results is mooring motions unrelated to the tides.

The weak semidiurnal tidal currents from the mooring device are qualitatively consistent with the literature (Pugh, 1987; Poulain et al., 2018) with ranges below 1 cm/s. Diurnal tides, especially the K1, are all above 1 cm/s near the surface, with fall currents averaging 2.2 cm/s. These might be attributed to the diurnal breeze, as alluded to before.

The most dominant tidal current found was the UPS1, with values reaching up to 5 cm/s. It is significant in all seasons and depths. This result possibly comes from the leakage of the near-inertial band and sensitivity to data set length. When taking larger datasets than the seasonal 90-day used here, such as 120-day and 180-day (not shown), we found this dominant frequency shifts away from the UPS1 tide and closer to 21.99 h, the inertial frequency at DeepLev. It is also evident that the signal found in rotary spectra done on the current time series shows the frequency as a predominantly clockwise motion (not shown).

DeepLev allowed the assessment of the criteria needed of surface drifters, in terms of temporal resolution, to give an adequate picture of a local tidal regime. The widely accepted Rayleigh criterion (further details in Thomson & Emery, 2014) of $\Delta f = \frac{1}{T}$ gives "just resolved" peaks, which, we argue in this paper, are contaminated due to leakage. The detailed findings in sections 3.2.2 and 3.3.1 illustrate this leakage in this local scenario. "Well resolved" peaks can be achieved with a constraint of $\Delta f > \frac{3}{2T}$. Although we have shown large amplitude changes when

641 analyzing different dataset lengths, only a few relevant drifters were available near DeepLev, a
642 serious impediment when adopting a stricter temporal constraint. All the results found by the
643 surface drifters, regardless of dataset length, were larger (>1 cm/s) than the results found in
644 moored datasets (<1 cm/s).

645

646 **Acknowledgments**

647 This study was supported by the Israeli Ministry of Science and the Italian Ministry of Foreign
648 Affairs.

649 **Open Research**

650 Data from the DeepLev Mooring site were used to create this manuscript, and all the code and
651 datasets needed to recreate the figures and results in this manuscript can be found at
652 10.5281/zenodo.7979160. The OSU TPXO Barotropic Tide Model was used, considering the
653 DeepLev mooring location (Lat= 33N03.67, Lon=34E29.296). The TPXO model was retrieved
654 using the TMD v 2.5 for Matlab (S. Erofeeva, L. Padman, and S. L. Howard (2020). Tide Model
655 Driver (TMD) version 2.5, Toolbox for Matlab
656 (https://www.github.com/EarthAndSpaceResearch/TMD_Matlab_Toolbox_v2.5), GitHub.
657 Retrieved [28.5.2023].). The current rose figure was made with Windrose version 200305
658 (Daniel Pereira (2023). Wind Rose
659 (https://www.mathworks.com/matlabcentral/fileexchange/47248-wind-rose), MATLAB Central
660 File Exchange. Retrieved May 28, 2023.). Tidal analysis was done using the T_Tide toolbox (R.
661 Pawlowicz, B. Beardsley, and S. Lentz, "Classical tidal harmonic analysis including error
662 estimates in MATLAB using T_TIDE", Computers and Geosciences 28 (2002), 929-937)
663 version 1.3b downloaded from https://www.eoas.ubc.ca/~rich/t_tide/t_tide_v1.3beta.zip. PSD
664 figures were produced and analyzed using the JLAB toolbox (Lilly, J. M. (2021), jLab: A data
665 analysis package for Matlab, v. 1.7.0, http://www.jmlilly.net/software).

Bathymetric Map of Eastern Mediterranian was created using M_Map (Pawlowicz, R., 2020. "M_Map: A mapping package for MATLAB", version 1.4m, [Computer software], available online at www.eoas.ubc.ca/~rich/map.html).

References

Albérola, C., Rousseau, S., Millot, C., Astraldi, M., Font, J., García-Lafuente, J., ... & Vangriesheim, A. (1995). Tidal currents in the western Mediterranean Sea. *Oceanologica Acta, 18(2),* pp.273-284. http://hdl.handle.net/10261/194257

Alford, M. H., MacKinnon, J. A., Simmons, H. L., & Nash, J. D. (2016). Near-inertial internal gravity waves in the ocean. *Annual review of marine science*, *8*, 95-123. http://dx.doi.org/10.1146/annurev-marine-010814-015746

Álvarez, O., Tejedor, B., Tejedor, L., & Kagan, B. A. (2003). A note on sea-breeze-induced seasonal variability in the K1 tidal constants in Cádiz Bay, Spain. *Estuarine, Coastal and Shelf Science*, *58*(4), 805-812. https://doi.org/10.1016/S0272-7714(03)00186-0

Arabelos, D. N., Papazachariou, D. Z., Contadakis, M. E., & Spatalas, S. D. (2011). A new tide model for the Mediterranean Sea based on altimetry and tide gauge assimilation. *Ocean Science*, *7*(3), 429-444. https://doi.org/10.5194/os-7-429-2011

Bendat, J. S., & Piersol, A. G. (2011). *Random data: analysis and measurement procedures*. Hoboken, NJ: John Wiley & Sons.

Carrère, L., Le Provost, C., & Lyard, F. (2004). On the statistical stability of the M2 barotropic and baroclinic tidal characteristics from along-track TOPEX/Poseidon satellite altimetry analysis. *Journal of Geophysical Research: Oceans*, *109*(C3). https://doi.org/10.1029/2003JC001873

Chavanne, C., Janeković, I., Flament, P., Poulain, P. M., Kuzmić, M., & Gurgel, K. W. (2007). Tidal currents in the northwestern Adriatic: High-frequency radio observations and numerical model predictions. *Journal of Geophysical Research: Oceans*, *112*(C3). https://doi.org/10.1029/2006JC003523

Cosoli, S., Drago, A., Ciraolo, G., & Capodici, F. (2015). Tidal currents in the Malta–Sicily Channel from high-frequency radar observations. *Continental Shelf Research*, *109*, 10-23. https://doi.org/10.1016/j.csr.2015.08.030

Deparis, V., Legros, H., & Souchay, J. (2013). Investigations of Tides from the Antiquity to Laplace. *Tides in astronomy and astrophysics*, 31-82. https://doi.org/10.1007/978-3-642-32961-6_2

Egbert, G. D., & Erofeeva, S. Y. (2002). Efficient inverse modeling of barotropic ocean tides. *Journal of Atmospheric and Oceanic Technology*, 19(2), 183-204. https://doi.org/10.1175/1520-0426(2002)019<0183:EIMOBO>2.0.CO;2

712 El-Geziry, T., & Radwan, A. (2012). Sea level analysis off Alexandria, Egypt. *The Egyptian*
713 *Journal of Aquatic Research*, *38*(1), 1-5. https://doi.org/10.1016/j.ejar.2012.08.004
714
715 El-Geziry, T. M. (2021). Sea-level, tides and residuals in Alexandria Eastern Harbour,
716 Egypt. *The Egyptian Journal of Aquatic Research*, *47*(1), 29-35.
717 https://doi.org/10.1016/j.ejar.2020.10.003
718
719 Ferrarin, C., Bellafiore, D., Sannino, G., Bajo, M., & Umgiesser, G. (2018). Tidal dynamics in
720 the inter-connected Mediterranean, Marmara, Black and Azov seas. *Progress in*
721 *Oceanography*, *161*, 102-115. https://doi.org/10.1016/j.pocean.2018.02.006
722
723 Feliks, Y., & Itzikowitz, S. (1987). Movement and geographical distribution of anticyclonic
724 eddies in the Eastern Levantine Basin. *Deep Sea Research Part A. Oceanographic Research*
725 *Papers*, *34*(9), 1499-1508. https://doi.org/10.1016/0198-0149(87)90105-1
726
727 Feliks, Y., Gildor, H., & Mantel, N. (2022). Intraseasonal oscillatory modes in the Eastern
728 Mediterranean Sea. *Journal of Physical Oceanography*. https://doi.org/10.1175/JPO-D-21-
729 0185.1
730
731 Garcia-Gorriz, E., Candela, J., & Font, J. (2003). Near-inertial and tidal currents detected with a
732 vessel-mounted acoustic Doppler current profiler in the western Mediterranean Sea. *Journal of*
733 *Geophysical Research: Oceans*, *108*(C5). https://doi.org/10.1029/2001JC001239
734

735 Gasparini, G. P., Smeed, D. A., Alderson, S., Sparnocchia, S., Vetrano, A., & Mazzola, S.
736 (2004). Tidal and subtidal currents in the Strait of Sicily. *Journal of Geophysical Research:*
737 *Oceans*, *109*(C2). https://doi.org/10.1029/2003JC002011
738
739 Hansen, D. V., & Poulain, P. M. (1996). Processing of WOCE/TOGA drifter data. *Journal of*
740 *Atmospheric and Oceanic Technology*, *13*(4), 900-909. https://doi.org/10.1175/1520-
741 0426(1996)013<0900:QCAIOW>2.0.CO;2
742
743 Hsieh, H. L., Fan, L. F., Chen, C. P., Wu, J. T., & Liu, W. C. (2010). Effects of semidiurnal tidal
744 circulation on the distribution of holo-and meroplankton in a subtropical estuary. *Journal of*
745 *Plankton Research*, *32*(6), 829-841. https://doi.org/10.1093/plankt/fbq026
746
747 Kar, S., Ghosh, I., Chowdhury, P., Ghosh, A., Aitch, P., Bhandari, G., & RoyChowdhury, A.
748 (2022). A model-based prediction and analysis of seasonal and tidal influence on pollutants
749 distribution from city outfalls of river Ganges in West Bengal, India and its mapping using GIS
750 tool. *PLOS Water*, *1*(2), e0000008. https://doi.org/10.1371/journal.pwat.0000008
751
752 Katz, T., Weinstein, Y., Alkalay, R., Biton, E., Toledo, Y., Lazar, A., ... & Herut, B. (2020). The
753 first deep-sea mooring station in the eastern Levantine basin (DeepLev), outline and insights into
754 regional sedimentological processes. *Deep Sea Research Part II: Topical Studies in*
755 *Oceanography*, *171*, 104663. https://doi.org/10.1016/j.dsr2.2019.104663
756

757 Khedr, A. M., Abdelrahman, S. M., & El-Din, K. A. A. (2018). Currents and sea level variability
758 of Alexandria coast in association with wind forcing. *Journal of King Abdulaziz*
759 *University*, *28*(2), 27-42. http://dx.doi.org/10.4197/Mar.28-2.3
760
761 Kwong, S. C., Davies, A. M., & Flather, R. A. (1997). A three-dimensional model of the
762 principal tides on the European shelf. *Progress in Oceanography*, *39*(3), 205–262.
763 https://doi.org/10.1016/S0079-6611(97)00014-1
764
765 Kunze, E. (1985). Near-inertial wave propagation in geostrophic shear. *Journal of Physical*
766 *Oceanography*, *15*(5), 544–565. https://doi.org/10.1175/1520-
767 0485(1985)015<0544:NIWPIG>2.0.CO;2
768
769 Lafuente, J. M. G., & Lucaya, N. C. (1994). Tidal dynamics and associated features of the
770 northwestern shelf of the Alboran Sea. *Continental Shelf Research*, *14*(1), 1-21.
771 https://doi.org/10.1016/0278-4343(94)90002-7
772
773 Lie, H. J., Lee, S., & Cho, C. H. (2002). Computation methods of major tidal currents from
774 satellite-tracked drifter positions, with application to the Yellow and East China Seas. *Journal of*
775 *Geophysical Research: Oceans*, *107*(C1), 3-1. https://doi.org/10.1029/2001JC000898
776
777 Lilly, J. M., 2021, jLab: A data analysis package for Matlab, v.1.7.1,
778 doi:10.5281/zenodo.4547006, http://www.jmlilly.net/software.
779

780 Lozano, C. J., & Candela, J. (1995). The M (2) tide in the Mediterranean Sea: Dynamic analysis
781 and data assimilation. *Oceanologica acta*, *18*(4), 419-441.
782
783 Medvedev, I. P., Vilibić, I., & Rabinovich, A. B. (2020). Tidal resonance in the Adriatic Sea:
784 Observational evidence. *Journal of Geophysical Research: Oceans*, *125*(8), e2020JC016168.
785 https://doi.org/10.1029/2020JC016168
786
787 Menna, M., Poulain, P. M., Bussani, A., & Gerin, R. (2018). Detecting the drogue presence of
788 SVP drifters from wind slippage in the Mediterranean Sea. *Measurement*, *125*, 447-453.
789 https://doi.org/10.1016/j.measurement.2018.05.022
790
791 Millot, C., & Garcia-Lafuente, J. (2011). About the seasonal and fortnightly variabilities of the
792 Mediterranean outflow. *Ocean Science*, *7*(3), 421-428.
793 https://doi.org/10.1016/j.measurement.2018.05.022
794
795 Müller, M., Cherniawsky, J. Y., Foreman, M. G., & von Storch, J. S. (2014). Seasonal variation
796 of the M 2 tide. *Ocean Dynamics*, *64*, 159-177. http://dx.doi.org/10.1007/s10236-013-0679-0
797
798 Naranjo, C., Garcia-Lafuente, J., Sannino, G., & Sanchez-Garrido, J. C. (2014). How much do
799 tides affect the circulation of the Mediterranean Sea? From local processes in the Strait of
800 Gibraltar to basin-scale effects. *Progress in Oceanography*, *127*, 108-116.
801 https://doi.org/10.1016/j.pocean.2014.06.005
802

803 Pastusiak, T. (2020). Hydrology of tidal waters at the glacier terminus and their Impact on
804 hydrographical surveys and navigation safety. *TransNav: International Journal on Marine*
805 *Navigation and Safety of Sea Transportation*, *14*(2). http://dx.doi.org/10.12716/1001.14.02.21
806
807 Pawlowicz, R., Beardsley, B., & Lentz, S. (2002). Classical tidal harmonic analysis including
808 error estimates in MATLAB using T_TIDE. *Computers & geosciences*, *28*(8), 929-937.
809 https://doi.org/10.1016/S0098-3004(02)00013-4
810
811 Pawlowicz, R., 2020. "M_Map: A mapping package for MATLAB", version 1.4m, [Computer
812 software], available online at www.eoas.ubc.ca/~rich/map.html
813
814 Percival, D. B., & Walden, A. T. (1993). *Spectral analysis for physical applications.* New York,
815 Cambridge University Press.
816
817 Perkins, H. (1976, November). Observed effect of an eddy on inertial oscillations. In *Deep Sea*
818 *Research and Oceanographic Abstracts* (Vol. 23, No. 11, pp. 1037–1042). Elsevier.
819 http://doi.org/10.1016/0011-7471(76)90879-2
820
821 Poulain, P. M., & Zambianchi, E. (2007). Surface circulation in the central Mediterranean Sea as
822 deduced from Lagrangian drifters in the 1990s. *Continental Shelf Research*, *27*(7), 981-1001.
823 https://doi.org/10.1016/j.csr.2007.01.005
824

825 Poulain, P. M., Menna, M., & Mauri, E. (2012). Surface geostrophic circulation of the
826 Mediterranean Sea derived from drifter and satellite altimeter data. *Journal of Physical*
827 *Oceanography*, *42*(6), 973-990. https://doi.org/10.1175/JPO-D-11-0159.1
828
829 Poulain, P. M., Bussani, A., Gerin, R., Jungwirth, R., Mauri, E., Menna, M., & Notarstefano, G.
830 (2013). Mediterranean surface currents measured with drifters: From basin to subinertial
831 scales. *Oceanography*, *26*(1), 38-47. http://dx.doi.org/10.5670/oceanog.2013.03
832
833 Poulain, P. M., & Centurioni, L. (2015). Direct measurements of W orld O cean tidal currents
834 with surface drifters. *Journal of Geophysical Research: Oceans*, *120*(10), 6986-7003.
835 https://doi.org/10.1002/2015JC010818
836
837 Poulain, P. M., Menna, M., & Gerin, R. (2018). Mapping Mediterranean tidal currents with
838 surface drifters. *Deep Sea Research Part I: Oceanographic Research Papers*, *138*, 22-33.
839 https://doi.org/10.1016/j.dsr.2018.07.011
840
841 Pugh, D.T. (1987). *Tides, surges and mean sea level.* New York, New York, John Wiley and
842 Sons
843
844 Ray, R. D. (2022). On seasonal variability of the M 2 tide. *Ocean Science*, *18*(4), 1073–1079.
845 https://doi.org/10.5194/os-18-1073-2022
846

847 Rosentraub, Z., & Brenner, S. (2007). Circulation over the southeastern continental shelf and
848 slope of the Mediterranean Sea: direct current measurements, winds, and numerical model
849 simulations. *Journal of Geophysical Research: Oceans*, *112*(C11).
850 https://doi.org/10.1029/2006JC003775
851
852 Sannino, G., Carillo, A., Pisacane, G., & Naranjo, C. (2015). On the relevance of tidal forcing in
853 modelling the Mediterranean thermohaline circulation. *Progress in Oceanography*, *134*, 304-
854 329. https://doi.org/10.1016/j.pocean.2015.03.002
855
856 Sammartino, S., García Lafuente, J., Naranjo, C., Sánchez Garrido, J. C., Sánchez Leal, R., &
857 Sánchez Román, A. (2015). Ten years of marine current measurements in E spartel Sill, Strait of
858 Gibraltar. *Journal of Geophysical Research: Oceans*, *120*(9), 6309-6328.
859 https://doi.org/10.1002/2014JC010674
860
861 Shaffer, B. (2011). Israel—New natural gas producer in the Mediterranean. *Energy Policy*, *39*(9),
862 5379–5387. https://doi.org/10.1016/j.enpol.2011.05.026
863
864 Slepian, D. (1978). Prolate spheroidal wave functions, Fourier analysis, and uncertainty—V: The
865 discrete case. Bell System Technical Journal, 5(5), 1371–1430. https://doi.org/10.1002/j.1538-
866 7305.1978.tb02104.x
867
868 Soto-Navarro, J., Lorente, P., Alvarez Fanjul, E., Carlos Sánchez-Garrido, J., & García-Lafuente,
869 J. (2016). Surface circulation at the Strait of Gibraltar: A combined HF radar and high resolution

model study. *Journal of Geophysical Research: Oceans*, 121(3), 2016-2034. https://doi.org/10.1002/2015JC011354

Thomson, D. J. (1982). Spectrum estimation and harmonic analysis. *Proceedings of the IEEE*, *70*(9), 1055–1096. https://doi.org/10.1109/PROC.1982.12433

Thomson, R. E., & Emery, W. J. (2014). *Data analysis methods in physical oceanography*. Newnes.

Tsimplis, M. N., Proctor, R., & Flather, R. A. (1995). A two-dimensional tidal model for the Mediterranean Sea. *Journal of Geophysical Research: Oceans*, *100*(C8), 16223–16239. https://doi.org/10.1029/95JC01671

Tsimplis, M. N., & Bryden, H. L. (2000). Estimation of the transports through the Strait of Gibraltar. *Deep Sea Research Part I: Oceanographic Research Papers*, *47*(12), 2219–2242. https://doi.org/10.1016/S0967-0637(00)00024-8

Ursella, L., Kovačević, V., & Gačić, M. (2014). Tidal variability of the motion in the Strait of Otranto. *Ocean Science*, *10*(1), 49-67. https://doi.org/10.5194/os-10-49-2014

Vilibić, I., Šepić, J., Dadić, V., & Mihanović, H. (2010). Fortnightly oscillations observed in the Adriatic Sea. *Ocean dynamics*, *60*, 57-63. https://doi.org/10.1007/s10236-009-0241-2

893 Wang, D., Pan, H., Jin, G., & Lv, X. (2020). Seasonal variation of the principal tidal constituents
894 in the Bohai Sea. *Ocean Science, 16*(1), 1-14. https://doi.org/10.5194/os-16-1-2020
895
896 Zaron, E. D., & Ray, R. D. (2017). Using an altimeter-derived internal tide model to remove
897 tides from in situ data. *Geophysical Research Letters, 44*(9), 4241–
898 4245. https://doi.org/10.1002/2017GL072950